Guiding and routing surface plasmons with transformation-invariant metamaterials

Huang, Yao; Zhang, Jingjing; Qiang, Bo; Xu, Zhengji; Wang, Qi Jie; Luo, Yu

2022

Huang, Y., Zhang, J., Qiang, B., Xu, Z., Wang, Q. J. & Luo, Y. (2022). Guiding and routing surface plasmons with transformation-invariant metamaterials. Journal of Optics, 24(1), 015003-. https://dx.doi.org/10.1088/2040-8986/ac38c5

https://hdl.handle.net/10356/156933

https://doi.org/10.1088/2040-8986/ac38c5

Guiding and Routing Surface Plasmons with Transformation-invariant Metamaterials

Yao Huang[1], Jingjing Zhang[2, *], Bo Qiang[1], Zhengji Xu[3,4], Qijie Wang[1, 5, ||] and Yu Luo[1, 6, #]

[1] School of Electrical and Electronic Engineering, Nanyang Technological University, 50 Nanyang Avenue, 639798, Singapore
[2] State Key Laboratory of Millimeter Waves, Southeast University, Nanjing 210096, China
[3] School of Microelectronics Science and Technology, Sun Yat-sen University, Zhuhai 519082, China
[4] Guangdong Provincial Key Laboratory of Optoelectronic Information Processing Chips and Systems, Zhuhai 519082, China
[5] School of Physical and Mathematical Sciences, Nanyang Technological University, 637371, Singapore
[6] UMI 3288 CINTRA, CNRS/NTU/THALES, Nanyang Technological University, 50 Nanyang Drive 637553, Singapore

E-mail: * zhangjingjing@seu.edu.cn
|| qjwang@ntu.edu.sg
luoyu@ntu.edu.sg

Received xxxxxx
Accepted for publication xxxxxx
Published xxxxxx

Abstract

Rough metallic surfaces cause severe scattering to surface plasmon polaritons (SPPs), thereby limiting the SPP transmission efficiency. Here, we propose a general scheme to design ultra-compact plasmonic routers that can confine and guide SPPs on arbitrarily shaped rough surface. Our strategy makes use of recently proposed transformation-invariant metamaterials. To illustrate the advantages of this approach, we perform finite-element simulations, showing that the performance of the designed surface-wave router is robust against the change in thickness. As a result, a λ/6-thick transformation-invariant metamaterial layer can significantly suppress scattering from arbitrarily shaped metallic bumps or crevices. We also give a blueprint to implement such ultracompact surface-wave routers based on periodic metal/ epsilon-near-zero (ENZ) material stackings.

Keywords: transformation optics, plasmonic, transformation-invariant metamaterial

Surface plasmon polaritons (SPPs) are propagating excitations, which are generated by the collective oscillation coupling of light and electrons on the metallic surface [1]. SPPs can be highly confined in a subwavelength domain, allowing for nanoscale light manipulation [2-9], engineered light-matter interaction, and other various applications in optical information technology [10, 11]. The composition and structure of the metal surface determine the SPPs characteristics.

SPP propagation in metallic nanostructures has been widely studied through both experiments and simulations. Nanostructures with various shapes have been proposed and constructed to guide and support SPP modes [12-21]. Owing to their ability to spatially confine electromagnetic waves at subwavelength scale, SPPs offer a feasible route to circumvent the diffraction limit and provide a potential guideline to deep miniaturization of optical components and circuits, which can be applied in communication, sensing, spectroscopy, etc. [22-23] SPPs remain non-radiating as long as the metal surface is translationally invariant along the propagation direction [12]. However, the SPP propagation is extremely sensitive to the metal surface configuration. Arbitrary roughness on the

metallic surface can cause significant scattering of the SPP waves, thereby deteriorating their energy guiding and confining performances. To solve this problem, transformation plasmonics was proposed [24-30]. It offers a route to suppress SPP scattering from the surface defect by engineering the refractive index of the surrounding background only. As a specific example, a surface wave adaptor designed with a bi-linear transformation was proposed to guide SPPs around a triangular bump or crevice [31]. However, the shape of such an adaptor is closely related to the birefringence of the composite anisotropic materials, and the realization of a compact adaptor requires extremely strong birefringence, which is difficult to attain with natural crystals or layered structures [32]. In addition, large birefringence will also lead to strong impedance-mismatch between the transformed medium and the free space, giving rise to additional scattering at the outer surface of the adapter.

Recently, inspired by the concept of the photonic doping [33], the transformation-invariant metamaterial (TIM) was proposed [34]. Such a metamaterial, also named as optical null medium [35], can be realized with stacked PEC and ENZ materials. TIM has two unique advantages, i.e., 1. its material parameters are preserved under arbitrary coordinate transformation; 2. Its impedance matches with free space for any incident angle. These properties make TIM a suitable candidate for the design of various ideal transformational optical devices [34,36].

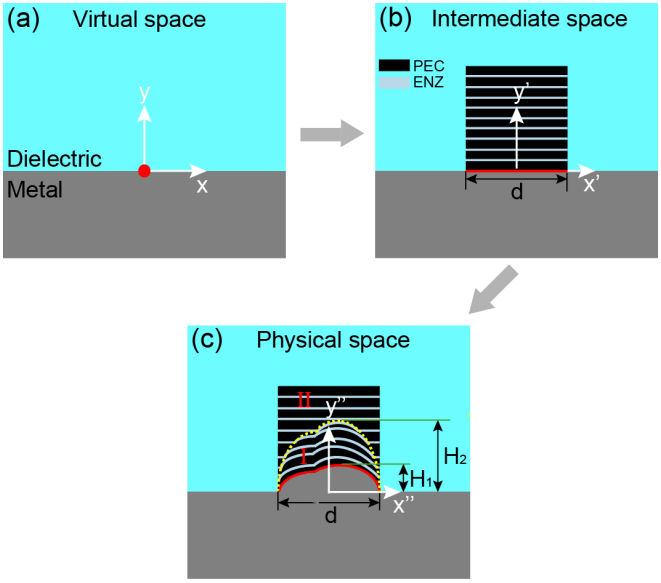

Fig. 1. Schematic of the SPP wave adaptor designed with transformation-invariant metamaterials. (a) The original space of a metal/dielectric interface with an infinitely small point located at the origin. (b) The intermediate space with highly anisotropic medium built with metal/ENZ stacking, where the red dot in (a) is transformed to the red straight line. (c) The physical space with highly anisotropic medium built with stacking of metal and ENZ material, where the red straight line in (b) is transformed to the bump, indicated by the red curve.

In this work, we apply TIM to design ultra-compact SPP wave adaptors, which can eliminate the SPP scattering brought by arbitrarily shaped surface defects. Compared with the previous approach based on transformation plasmonics, our scheme enables the surface-wave adaptor to be realized with an ultrathin layer of TIM. Specifically, we compare our TIM-based surface wave adaptor with previous designs using bilinear transformations, showing that the performance of our device is quite robust against variations in the TIM thickness. Our design is general and not restricted to the specific examples we discussed in this paper. It can be applied to guiding and routing of SPPs around arbitrarily shaped defects and corners.

Our general design scheme is illustrated in Fig. 1, which depicts the coordinate transformation used to achieve the surface wave adaptor for an arbitrarily shaped bump on the metal/dielectric interface. An infinitely small points indicated by red dot in Fig. 1(a) can be transformed to the red straight line in Fig. 2(b), through the following coordinate transformation

$$x' = \infty \cdot x, y' = y, z' = z \tag{1}$$

where (x, y, z) and (x', y', z') correspond to the virtual space and the intermediate space, respectively. In this way, a stretched slab region in the Fig. 1(b) will obtain the permittivity and permeability written as

$$\varepsilon' = \varepsilon_0 \begin{pmatrix} A & 0 & 0 \\ 0 & B & 0 \\ 0 & 0 & B \end{pmatrix}, \mu' = \mu_0 \begin{pmatrix} A & 0 & 0 \\ 0 & B & 0 \\ 0 & 0 & B \end{pmatrix} \tag{2}$$

, where A = ∞, B = 0. According to the effective medium theory, such highly anisotropic material parameters can be realized with periodic multilayered structures consisting of metals and ENZ materials as indicated by the black slabs and light blue slits in Fig. 1(b), respectively. Our SPP adapter is obtained through a space compression along the vertical y direction,

$$x'' = x', y'' = af(x') + by', z'' = z' \tag{3}$$

where (x', y', z') and (x'', y'', z'') correspond to the intermediate space and the physical space, respectively, the red straight line in Fig. 1(b) is transformed into the red curve in Fig. 1(c). For p-polarized SPP waves, the material parameters of the transformed medium (the region between the yellow dashed line and red curve in Fig. 1(c)) can be deduced as

$$\varepsilon'' = \frac{\varepsilon_0}{|J|} \begin{pmatrix} A + Ba^2 \left(\frac{df(x')}{dx'} \right)^2 & Bab \frac{df(x')}{dx'} \\ Bab \frac{df(x')}{dx'} & Bb^2 \end{pmatrix}, \mu'' = B \frac{\mu_0}{|J|} = 0 \tag{4}$$

The permittivity matrix can be diagonalized through coordinate rotation. Since A = ∞, B = 0, the principal values of ε" are kept unchanged, i.e.

$$\varepsilon'' = \begin{pmatrix} \infty & 0 \\ 0 & 0 \end{pmatrix} \quad (5)$$

while the principal axis is orientated along the $\hat{x} + f'(x)\hat{y}$ direction. In other words, the optical axis of the transformed medium is everywhere conformal to the boundary of the surface defect indicated by the red curve in Fig.1(c). Such highly anisotropic medium in our design can be achieved through multilayered metallodielectric structures consisting of two regions, i.e. region I where the metal (black area) and ENZ (light blue area) layers are everywhere conformal to the boundary of the surface defect and region II where the metal and ENZ slabs are orientated along the horizontal direction. To make our discussions applicable to any frequency range, we set the heights of the surface defect and the adaptor as H_1 and H_2, respectively and defines the thickness of the adaptor as = H_2 - H_1 .

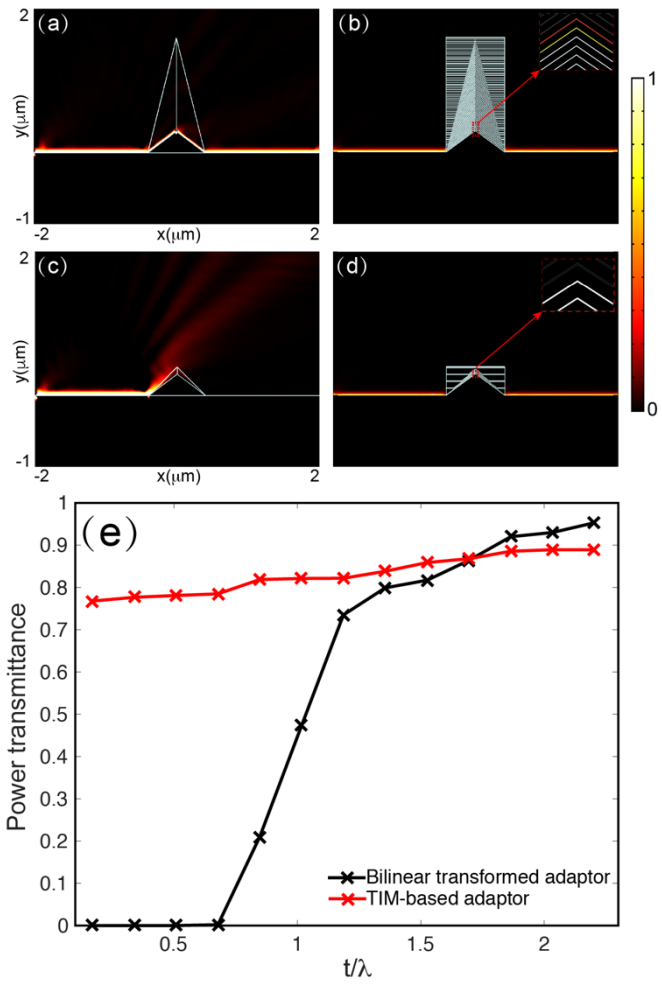

Fig. 2. Power flow when SPPs propagate on a triangular bump covered by a plasmonic adapter designed with (a, c) a bilinear transformation and (b, d) transformation-invariant metamaterials. In (a, b), the heights of the bump and the adapter are set as $H_1 = 0.51\lambda$ and $H_2 = 2.71\lambda$, respectively, while in (c, d), they are set as $H_1 = 0.51\lambda$ and $H_2 = 0.68\lambda$, respectively. (e) The power transmittance of the bilinear plasmonic adaptor and the TIM-based adaptor in this paper versus the normalized adaptor thickness t ranging from 0.17 to 2.21.

As mentioned before, the TIM-based SPP adapter has the advantage that its performance is robust against thickness variations, i.e. changes in H_2. To illustrate this point, we compare the power flows of SPPs along the bumped metallic surface covered by our TIM-based adaptors and the conventional TO-based adaptors designed with a bilinear transformation [31]. The background material is assumed to be silicon nitride, with a permittivity $\varepsilon_b = 4.67$. The surface defect has a triangular shape with 0.51λ in height and 1.36λ in width. An electric point dipole located at the metal/dielectric interface is applied to excite the surface plasmon on the metallic surface. We compare the simulated power flow for two different adapter heights, i.e., $H_2 = 2.71\lambda$ (corresponding to a normalized thickness $t \approx 8\lambda/3$) and $H_2 = 0.68\lambda$ (corresponding to a normalized thickness $t \approx \lambda/6$). For the large adapter height $H_2 = 2.71\lambda$ shown in Fig. 2(a) and (b), both TIM-based adaptors and the bi-linear transformed one can successfully guide SPPs around the bump without scattering. On the contrary, when the adaptor height is reduced to $H_2 = 0.68\lambda$, only the TIM-based adapter can still restore the SPP propagation (see Fig. 2(d)), whilst the bilinear transformed one induces large scattering due to strong impedance mismatch between the adapter and the background medium. Insets in Fig. 2 (b) and (d) plot the power flow distributions in the TIM layers.

To further illustrate the performance of the designed adapter against the thickness variation, we plot in Fig. 2(e) the power transmission at different adapter thicknesses. The power transmission is calculated as $\eta = P_1/P_2$, where P_1 and P_2 represent the power at x = 3.05λ (i.e. 2.37λ behind the adapter) and x = -3.05λ (i.e. 2.37λ in front of the adapter), respectively. As depicted by the red curve in Fig. 2(e), transmission from our TIM-based adaptor remains a constant larger than 70% over the entire range of adapter thickness t = 0.17λ to 2.21λ. Such a property results from the unchanged impedance $\mu_z/\varepsilon_y = \mu_0/\varepsilon_0$ which is matched to the background medium irrespective of the adapter thickness. On the contrary, the bilinear adapter designed with transformation plasmonics leads to efficient power transmission only when $t > 1.19\lambda$, as indicated by the black curve. The power transmission drops sharply from 70% to 20% when t decreases from 1.19λ to 0.68λ and remains nearly zero for $t < 0.51\lambda$. It is worth noticing that in the computation of Fig. 2(e), the bilinear adaptor is made of homogenous effective medium irrespective of the anisotropy, while our TIM-based adapter is implemented with periodic metal/ENZ structure which unavoidably leads to finite scattering owing to finite structural period. Hence, the transmittance of the TIM-based design is

slightly lower than that of the bi-linear one for $t > 1.69\lambda$. This does not necessarily mean that the performance of our design is poorer at large adapter thickness. If homogeneous metamaterials are applied in the simulation, the transmission efficiency of the TIM-based adapter will be close to 1.

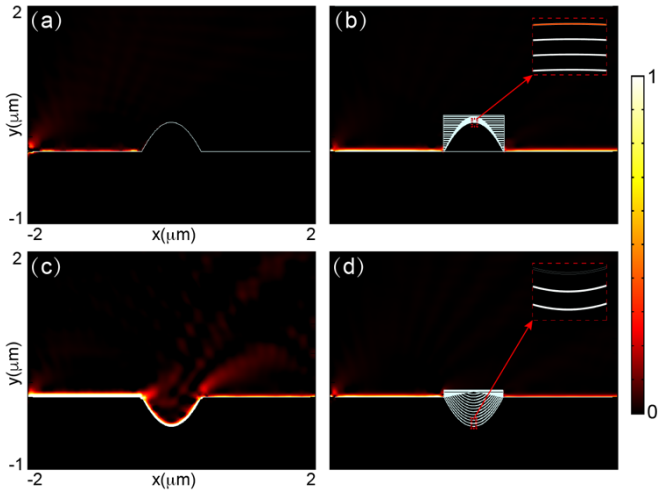

Fig. 3. Power flow when SPPs propagate on (a) a bare parabolic protrusion, (b) a parabolic protrusion covered by judiciously designed TIM, (c) a parabolic crevice, (d) a parabolic crevice covered by judiciously designed TIM. In (a, b), the heights of the bump and the adapter are set as $H_1 = 0.68\lambda$ and $H_2 = 0.85\lambda$, respectively, while in (c, d), they are set as $H_1 = -0.68\lambda$ and $H_2 = 0.17\lambda$, respectively.

Another advantage of our approach is that it can be applied to guide SPPs around the arbitrarily shaped surface imperfections. To illustrate this point, we consider two cases, the first design is used to confine SPPs along a parabolic protrusion (0.68λ in height, 1.36λ in width), and the second one serves to route SPPs around a parabolic crevice (0.68λ in depth, 1.36λ in width) of a similar shape. The contours of the protrusion and crevice are given by $y = -x^2/0.68\lambda + 0.68\lambda$ and $y = x^2/0.68\lambda - 0.68\lambda$, respectively. As shown in Fig. 3, our TIM-based designs can significantly suppress the scattering from the protrusion/crevice and successfully restore SPP propagation on the other side of the metal surface. Insets in Fig. 3(b) and (d) show how the energy is guided around the protrusion/crevice by the TIM.

As a final remark, we highlighted that this TIM-based scheme is general and can even be applied to route SPPs around a sharp surface corner. This point is demonstrated by Fig. 4, where we compare the magnetic field intensity distribution when SPPs pass through a 90° sharp corner without (Fig. 4(a)) and with (Fig. 4(b)) the TIM-based router. Such a router is designed with a proper combination of two pieces of TIMs, one with the optical axis along the horizontal direction (i.e. region I in Fig. 4(b)), the other with the optical axis along the vertical direction (i.e. region II in Fig. 4(b)). In both regions, the thicknesses of the metal and ENZ slits are fixed as $d_{\text{metal}} = 0.03\lambda$ and $d_{\text{ENZ}} = 0.003\lambda$. Our results show that the sharp corner with 90° bending angle triggers severe scattering (in Fig. 4(a)), which, on the contrary, is significantly suppressed by our TIM-based router (in Fig. 4(b)). The propagation of the SPP wave has been successfully restored at the vertical metal surface after passing through the router. Since the TIM-based router conceals the square region in Fig. 4(b), SPPs propagate around the sharp corner as if they are propagating along a flat metal surface. The inset in Fig. 4(b) illustrates how the energy of SPP is bent by 90° slits.

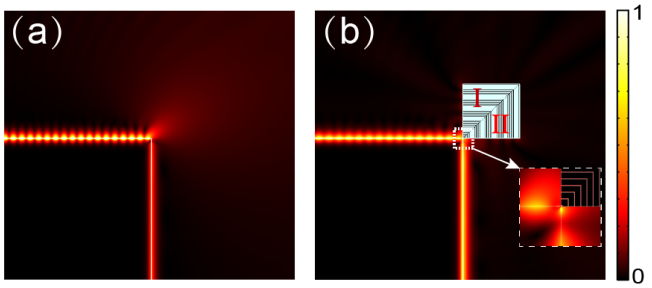

Fig. 4. Simulated magnetic field when SPPs propagate on (a) a bare 90°-bended metal corner and (b) a 90°-bended metal corner covered by transformation-invariant metamaterial-based wave adaptor.

To conclude, we propose a general design scheme of plasmonic wave adaptor that suppresses the SPP scattering produced by the arbitrarily shaped metallic surface imperfection. In contrast to the bilinear transformed surface wave adaptor that only works well with large adaptor thickness, our proposed plasmonic wave adaptor shows robust performance to the thickness variation and offers effective elimination to the defect-induced scattering when the thickness of the adaptor is as small as $t \approx \lambda/6$. Furthermore, two plasmonic adaptors that target to conceal the parabola-shape bump/crevice and a plasmonic router that adopted to guide waves along a 90°-bended metal corner are also proposed to validate the versatility of our proposal. Our method has potential applications in the SPP signal transmission technology and may provide guidelines for optical device designs which requires the manipulation of light trajectory in all frequency ranges.

Acknowledgements

This work was sponsored by Singapore Ministry of Education (No. MOE2018-T2-2-189 (S) and MOE2018-T2-1-176), A*Star AME IRG grant (No. A20E5c0095), Programmatic Funds (No. A18A7b0058), National Research Foundation Singapore Competitive Research Program (No. NRF-CRP22-2019-0006 and NRF-CRP23-2019-0007).

References

[1] S. A. Maier, Plasmonics: Fundamentals and Applications (Springer, 2007).
[2] M. L. Juan, M. Righini, and R. Quidant, Nat. Photonics 5, 349 (2011).
[3] S. Nie and S. R. Emory, Science 275, 1102 (1997).
[4] S. Kim, J. Jin, Y. J. Kim, I. Y. Park, Y. Kim, and S. W. Kim, Nature 453, 757 (2008).
[5] P. Genevet, J. P. Tetienne, R. Blanchard, M. A. Kats, J. B. Müller, M. O. Scully, and F. Capasso, Appl. Opt. 50, G56 (2011).
[6] H. J. Lezec, J. A. Dionne, H. A. Atwater, Science 316, 430 (2007).
[7] T. Kosako, Y. Kadoya and H. F. Hofmann, Nat. Photonics 4, 312 (2010).
[8] N. Yu, P. Genevet, M. A. Kats, F. Aieta, J. P. Tetienne, F. Capasso, and Z. Gaburro, Science, 334, 333 (2011).
[9] N. Yu, Q. Wang and F. Capasso, Laser Photonics Rev. 6, 24 (2012).
[10] E. Ozbay, Science 311, 189 (2006).
[11] M. L. Brongersma and V. M. Shalaev, Science 328, 440 (2010).
[12] E. N. Economou, Phys. Rev. 182, 539 (1969).
[13] J. Takahara, S. Yamagishi, H. Taki, A. Morimoto, and T. Kobayashi, Opt. Lett. 22, 475 (1997).
[14] K. V. Nerkararyan, Phys. Lett. A, 237, 103 (1997).
[15] D. E. Chang, A. S. Sorensen, E. A. Demler and M. D. A. Lukin, Nat. Phys. 3, 807 (2007).
[16] D. F. P. Pile, D. K. Gramotnev, R. F. Oulton and X. Zhang, Opt. Express, 15, 13669 (2007).
[17] R. F. Oulton, D. F. P. Pile, Y. M. Liu, and X. Zhang, Phys. Rev. B, 76, 035408(2007).
[18] J. Elser and V. A. Podolskiy, Phys. Rev. Lett. 8, 100, 066402(2008).
[19] B. Baumeier, T. A. Leskova, A. A. Maradudin, Phys. Rev. Lett. 103, 246803(2009).
[20] A. L. Falk, F. H. L. Koppens., C. L.Yu, K. Kang, N. de Leon Snapp, A. V. Akimov, M.-H. Jo, M. D. Lukin, and H. Park, Nat. Phys. 5, 475 (2009).
[21] D. K. Gramotnev, S. I. Bozhevolnyi, Nat. Photonics 4, 83 (2010).
[22] W. L. Barnes, A. Dereux, and T. W. Ebbesen, Nature 424, 824 (2003).
[23] E. Ozbay, Science 311, 189 (2006).
[24] A. J. Ward, J. B. Pendry, J. Mod. Opt. 43, 773 (1996).
[25] U. Leonhardt, Science 312, 1777 (2006).
[26] H. Chen, C. T. Chan, and P. Sheng, Nat. Mater. 9, 387 (2010).
[27] J. Zhang, J. B. Pendry, and Y. Luo, Adv. Photonics. 1, 014001(2019).
[28] P. A. Huidobro, M. L. Nesterov, L. Martin-Moreno, and F. J. Garcia-Vidal, Nano Lett. 10, 1985–1990 (2010).
[29] Y. Liu, T. Zentgraf, G. Bartal, and X. Zhang, Nano Lett. 10,1991(2010).
[30] A. Aubry, D. Y. Lei, A. I. Fernández-Domínguez, Y. Sonnefraud, S. A. Maier, and J. B. Pendry, Nano Lett. 10, 2574 (2010).
[31] J. Zhang, S. Xiao, M. Wubs and N. A. Mortensen, Acs. Nano. 5(6), 4359-4364(2011).
[32] J. Zhang, L. Liu, Y. Luo, S. Zhang, and N. A. Mortensen, Opt. Express 19, 8625 (2011).
[33] I. Liberal, A. M. Mahmoud, Y. Li, B. Edwards, and N. Engheta, Science 355, 1058(2017).
[34] Y. M. Zhang, Y. Luo, J. B. Pendry, and B. L. Zhang, Phys. Rev. Lett. 123, 067701 (2019).
[35] F. Sun and S. He, Sci. Rep. 5, 16032 (2015).
[36] F. B. Yang, B. Y. Tian, L. J. Xu, and J. P. Huang, Phys. Rev. Appl. 14, 054024 (2020).